ARTICLE

ACS chemical biology

Structural Basis for Binding Specificity between Subclasses of Modular Polyketide Synthase Docking Domains

Tonia J. Buchholz[†], Todd W. Geders[‡], Frank E. Bartley III[‡], Kevin A. Reynolds[§], Janet L. Smith[‡], and David H. Sherman[†,*]

[†]Life Sciences Institute, Departments of Medicinal Chemistry, Chemistry, and Microbiology & Immunology, University of Michigan, Ann Arbor, Michigan 48109, [‡]Life Sciences Institute, Department of Biological Chemistry, University of Michigan, Ann Arbor, Michigan 48109, and [§]Department of Chemistry, Portland State University, Portland, Oregon 97207

ABSTRACT Bacterial type I polyketide synthases (PKSs) assemble structurally diverse natural products of significant clinical value from simple metabolic building blocks. The synthesis of these compounds occurs in a processive fashion along a large multiprotein complex. Transfer of the acyl intermediate across interpolypeptide junctions is mediated, at least in large part, by N- and C-terminal docking domains. We report here a comprehensive analysis of the binding affinity and selectivity for the complete set of discrete docking domain pairs in the pikromycin and erythromycin PKS systems. Despite disconnection from their parent module, each cognate pair of docking domains retained exquisite binding selectivity. Further insights were obtained by X-ray crystallographic analysis of the PikAIII/PikAIV docking domain interface. This new information revealed a series of key interacting residues that enabled development of a structural model for the recently proposed H2-T2 class of polypeptides involved in PKS intermodular molecular recognition.

Although naturally occurring polyketides have a wide variety of chemical structures, they are produced by three broad classes of polyketide synthases (PKSs) that share a common mechanism. This involves sequential decarboxylative condensation reactions to form carbon−carbon bonds between simple carboxylic acid extender units (*1, 2*). Type I modular PKSs are the large, multifunctional enzymes responsible for the production of a diverse family of structurally rich and often biologically active natural products (*e.g.*, antimicrobial, antifungal, antiviral, anticancer, and immunosuppressant compounds) (*1, 3*). Recently, structural studies have provided important new insights relating to the architecture and mechanism of type I PKSs and the related fatty acid synthases (*4*–*7*). Found in a variety of bacteria, modular PKSs direct biosynthesis *via* covalently linked catalytic domains that are organized into linear modules where each module houses the requisite catalytic domains to perform a single elongation step in the building of the polyketide chain (Figure 1, panels a and b). Each elongation module receives the nascent chain from the previous module, extends the polyketide by two carbons, and (typically) modifies this portion before passing the intermediate to the downstream PKS protein (*5, 8*). The final chemical structure is determined by the number of modules in the pathway, their catalytic domain composition, and arrangement in the biochemical assembly line (Figure 1, panels a and b). Extensive research has identified signature amino acid sequences within the catalytic domains that guide substrate specificity (*5, 9*). However, details about the protein−protein interactions that gov-

*Corresponding author, davidhs@umich.edu.

Received for review October 23, 2008 and accepted December 12, 2008.

Published online January 16, 2009

10.1021/cb8002607 CCC: $40.75

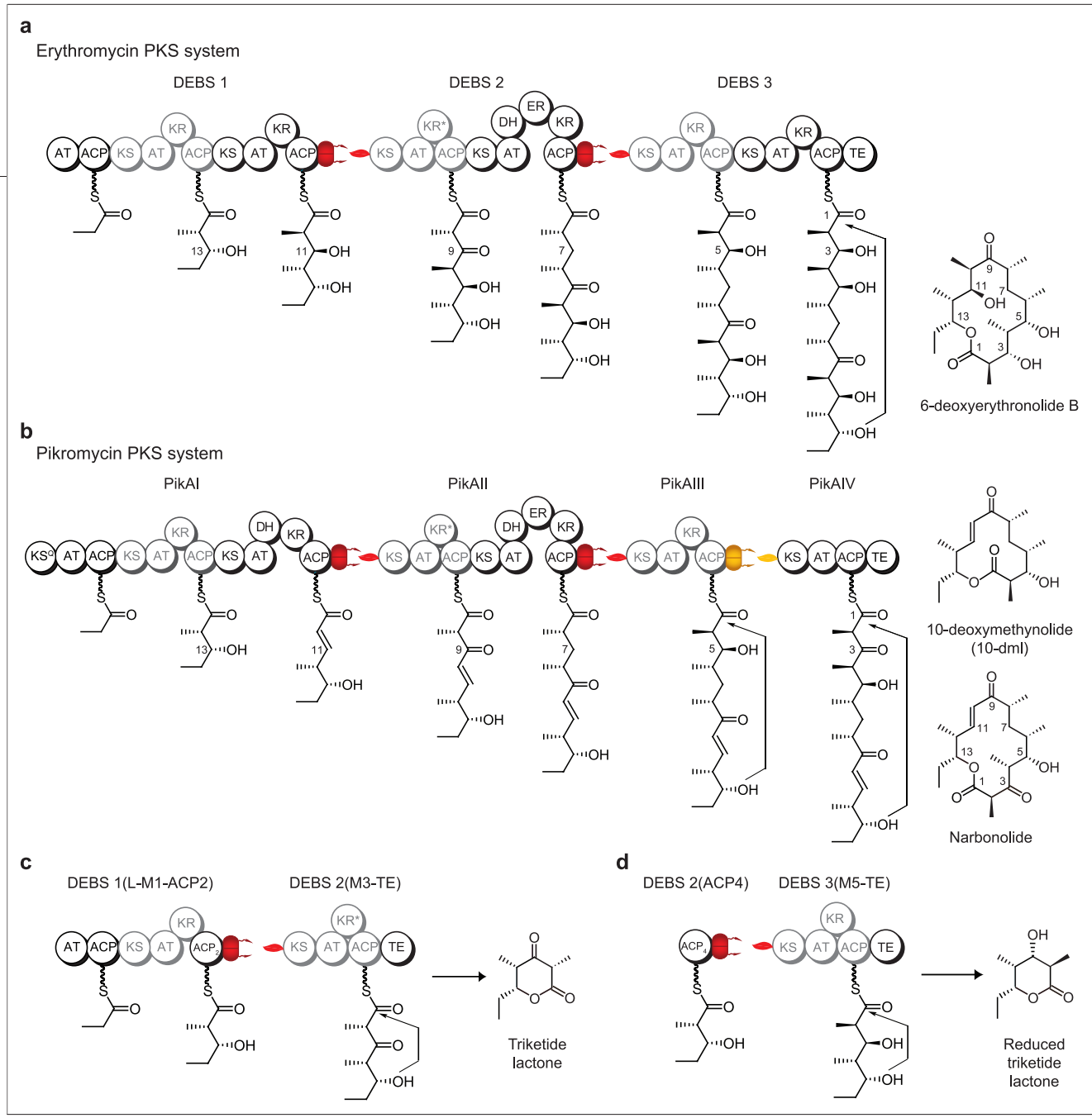

Figure 1. Type I polyketide synthases. a,b) Arrangement of the PKS portions of the pikromycin and erythromycin biosynthetic pathways and their macrolactone products. c,d) Two examples of the intermodular transfer and elongation assays featuring the erythromycin PKS system (*19*–*22*). Abbreviations: ACP, acyl carrier protein; AT, acyltransferase; DH, dehydratase; ER, enoyl reductase; KR, ketoreductase; KS, ketosynthase; KS^Q, decarboxylative ketosynthase; TE, thioesterase. Docking domains are colored by proposed subclass; H1-T1 are red, and H2-T2 is gold. Domain sizes are not drawn to scale.

ern acyl transfer between modules have only recently been explored (*10*–*12*).

The modular nature of type I PKSs has led many to envision rational "mix and match" bioengineering for the generation of novel polyketide products. As such, metabolic engineering or combinatorial biosynthesis has emerged as one potential route to create novel polyketide agents (*13*–*16*). Specific changes can be introduced to the final polyketide core in a controlled fashion by manipulating the genes that encode modular PKSs. Modifications at the level of the modules or the individual catalytic domains within a PKS module have been used to generate hundreds of novel polyketide structures, thereby establishing the potential of these applications (*13*–*17*). However, engineered PKS modules often fail to produce significant quantities of the desired product (*17*). Fundamental studies to establish the mechanistic basis for efficient molecular interac-

tions between PKS multifunctional proteins will likely facilitate effective design and assembly of productive bioengineered pathways. The importance of this new information motivated the studies described in this report.

The fidelity and efficiency of acyl transfer at the interfaces of the individual PKS proteins is thought to be governed by helical regions, termed docking domains (dd), located at the C-terminus of the upstream and N-terminus of the downstream polypeptide chains (Figure 1, panels a and b) (*18*). Two main strategies have been employed to study the specificity determinants for interpolypeptide (*e.g.*, module→module) communication. In the first strategy, modules (or excised domains) from the erythromycin PKS system were used to create a variety of *in vitro* intermodular transfer and elongation assays (see Figure 1, panels c and d) (*19*–*22*). Typically, a variety of chimeric proteins were generated to investigate the effect of matched or mismatched docking domains in combination with a series of ACP/KS pairings. Detection of triketide lactones resulting from the transfer and elongation of diketide intermediates established that complementary docking domain pairs are required for efficient transfer of polyketide intermediates between polypeptides (*11, 23*). In some cases, formation of the cognate ACP and KS pairs also appears to impart a catalytic advantage, although tolerance for mispairing at this junction is also evident (*19, 20*).

The second strategy for analysis of PKS module–module molecular recognition has been to structurally characterize the docking interface. A docking domain complex model for the DEBS 2/DEBS 3 interface (Figure 1, panel a) was developed *via* protein NMR spectroscopy (*18*). The structure established that the docking domains are helical and revealed two roles for the C-terminal PKS docking domain (ACP-side docking domains, ACPdd). First, this region appears important for stabilizing the PKS homodimer. Second, ACPdd is poised to interact with the downstream KS polypeptide through its terminal helix. The N-terminal PKS docking domain (KS-side docking domain, KSdd) exhibits a coiled-coil motif that has been observed both in the solution structure of the fused DEBS 2/DEBS 3 construct (*18*) and subsequently in the X-ray crystal structure of the DEBS 3 KS-AT didomain (*6*). The KSdd dimer presents a small hydrophobic patch, sometimes flanked by charged residues, as a narrow binding groove where the ACPdd terminal helix can bind.

Extension of the current DEBS 2/DEBS 3 structural model to the full range of docking domains across modular PKSs has not been possible because of low sequence similarity for a large subset of sequences. However, in a recent report based on the DEBS 2/DEBS 3 structural model and computational analysis of docking domain sequences from 42 characterized PKS systems, Thattai *et al.* (*24*) proposed a new organization of PKS docking domains into distinct subclasses. On the basis of this classification system, the majority of docking domains (including the structurally characterized DEBS2/DEBS3 pair) fall into a single group termed H1-T1 (for head 1 and tail 1). Until this report, there was no structural information available for the proposed H2-T2 group of PKS docking domains.

To develop further our understanding of docking domain interactions in modular PKSs and to expand fundamental information about docking domain protein structure, we pursued both biochemical and structural characterization of docking domains from two well-studied PKS biosynthetic systems. First, we report an analysis of the binding affinities of discrete docking domain pairs excised from the erythromycin (DEBS) and pikromycin (Pik) PKSs, using surface plasmon resonance and fluorescence polarization methods. In addition, we report the first X-ray crystal structure of a member of the recently proposed H2-T2 class of PKS docking domains, derived from the interface between PikAIII (module 5) and PikAIV (module 6) proteins from the Pik PKS system (Figure 1, panel b) (*25*). Combining structural characterization of the PikAIII/PikAIV interface with discrete docking domain affinity measurements, we provide evidence in support of the prevailing model wherein the binding specificity that determines the linear arrangement of proteins in the biosynthetic assembly line is encoded in these small, terminal peptide sequences. Finally, we present a model for the observed docking domain specificity across a matrix of interacting pairs from the pikromycin and erythromycin pathways.

RESULTS AND DISCUSSION

Binding Affinities of Discrete Docking Domains *via* Surface Plasmon Resonance. To test the capacity of discrete docking domains to discriminate between possible partners within a single biosynthetic pathway

and/or between related pathways, we produced peptides corresponding to each ACPdd and KSdd region of the pikromycin and erythromycin PKS pathways (Figure 1, panels a and b). Peptides were overexpressed in *E. coli* and purified using a His_6-affinity handle followed by removal of the His-tag *via* TEV protease cleavage where necessary. While each of the docking domain constructs resulted in stable, soluble protein, the yields of the PikAII KSdd and PikAIII KSdd were low. Hence, for these two peptides, chemical synthesis was employed to produce larger quantities. The ability of KSdd's to bind native immobilized ACPdd partners was evaluated using surface plasmon resonance (SPR). Biosensors based on SPR technology have been used to measure binding interactions across a wide range of affinities between partners (including discrete docking domains from a related mixed PKS/NRPS megasynthase system) varying from small molecules to large protein complexes (*26–28*). In modular PKSs, individual docking domains are identifiable by considering sequences directly downstream from the ends of the C-terminal ACP domain or directly upstream from the conserved start sites of the N-terminal KS domain. Using multiple sequence alignments of a number of characterized type I PKS systems, we designed, overexpressed, and purified (and in two cases synthesized) a complete set of discrete ACPdd's and KSdd's from the erythromycin and pikromycin system (Supplementary Figure 1). In these studies, we used a noncovalent method to immobilize the N-terminally His-tagged ACPdd's to a nickel-loaded NTA sensor chip (Figure 2, panel a) (*29*). The measured affinity (K_D) of His-tagged PikAIII ACPdd to the nickel-NTA surface was 4.0 $\pm$ 0.04 nM (Supplementary Figure 2). This binding was sufficiently tight to enable measurement of the desired ACPdd−KSdd interactions when paired with tagless KSdd's in solution.

After immobilization of ACPdd, equilibrium analysis of a variety of matched or mismatched docking domain pairs was performed using sequential injections of KSdd at varying concentrations. Using docking domains from the erythromycin and pikromycin PKSs, we measured K_D's for the matched docking domain pairs between 70−130 μM (Figure 2). Additionally, we were able to calculate individual kinetic parameters for the PikAIII/PikAIV binding pair ($k_{on} = 3000 \pm 1800\ M^{-1}\ s^{-1}$, $k_{off} = 0.21 \pm 0.03\ s^{-1}$, $K_D = 73 \pm 43$ μM) (Supplementary Figure 3) that were in good agreement with the equilibrium analysis. As a negative control, a PikAIII ACPdd construct lacking the final nine amino acids was unable to bind to its partner KSdd (PiKAIV) or any other KSdd's. A similar C-terminal deletion of the PikAIII ACPdd was recently shown to be incompetent for production of narbonolide in an *in vitro* PikAIII/PikAIV chemoenzymatic system (*30*). Furthermore, studies with mismatched docking domains clearly demonstrate that the ability to discriminate between potential PKS protein partners is encoded within the docking domains themselves (Supplementary Figure 4).

Ultimately, docking domains function not as discrete peptides but as small appendages on much larger proteins (Figure 1). In addition to testing the complete library of discrete ACPdd's and KSdd's from the pikromycin and erythromycin PKS systems, we extended our analysis of the PikAIII/PikAIV docking interface to the neighboring domains. Assigning affinity and specificity determinants to (i) the docking domains, (ii) the neighboring catalytic domains, (iii) the phosphopantetheine arm, and (iv) the growing polyketide chain will begin to separate the importance of the correct protein−protein interaction from the questions of substrate specificity at the catalytic centers. Although binding of a larger KSdd-containing protein (PikAIV KSdd-KS-AT) to the His-tag immobilized PikAIII ACPdd *via* SPR was observed, we were unable to calculate affinity values because of the high background refractive index change exhibited. We thus sought an alternative method to address this question.

Binding Affinities of Discrete Docking Domains *via* Fluorescence Polarization. To assess the effect of larger protein complexes on docking domain binding affinity, a fluorescence polarization (FP) assay was employed (*31*). We empirically determined the best fluorophore placement through the addition of a cysteine residue at each of the four possible termini (N-terminus and C-terminus of PikAIII ACPdd and PikAIV KSdd). Inclusion of a single cysteine residue enabled site-specific labeling with iodoacetamide-BODIPY-FL. Titration of increasing concentrations of the unlabeled matched docking domain identified the C-terminus of PikAIII ACPdd (termed PikAIII ACPdd-FL) as the optimal fluorophore placement, as this tracer exhibited the largest change in FP upon protein binding. The binding affinity of the PikAIV KSdd for PikAIII ACPdd-FL measured using this method provided an independent confirmation of the discrete docking domain binding affinities generated using SPR (Figure 3). When the larger KSdd-containing PikAIV proteins were titrated against ACPdd-

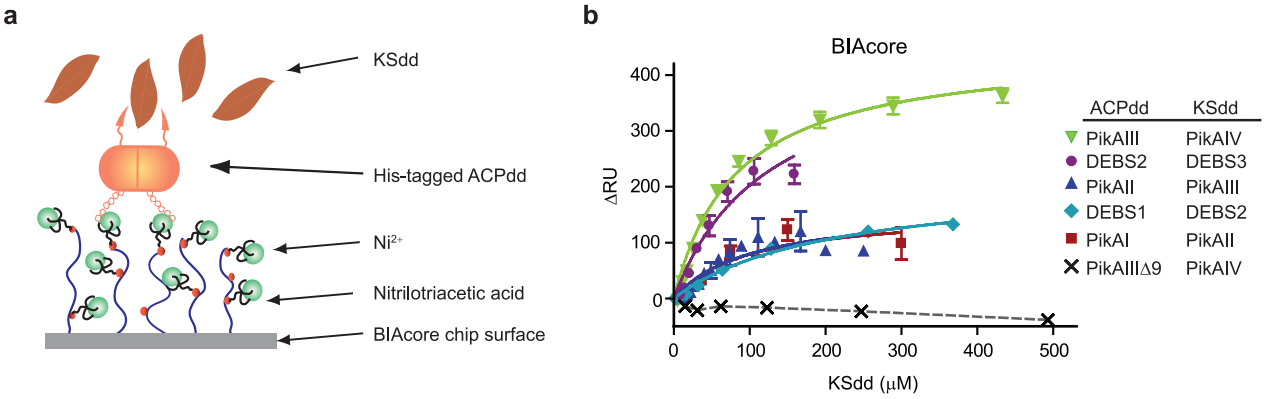

c

ACPdd's \ KSdd's	PikAII	PikAIII	PikAIV	DEBS2	DEBS3
PikAI	120 ± 35 μM	NB	NB	NB	NB
PikAII	NB	110 ± 26 μM	NB	NB	NB
PikAIII	NB	NB	70 ± 11 μM	NB	NB
DEBS1	NB	NB	NB	110 ± 6 μM	NB
DEBS2	NB	NB	NB	NB	130 ± 50 μM
PikAIIIΔ9	NB	NB	NB	NB	NB

Figure 2. Binding analysis of discrete ACPdd's to matched and mismatched KSdd's measured by SPR. a) SPR assay design: after immobilizing the ACPdd's *via* their His-tags, varying concentrations of discrete KSdd's were injected over the ACPdd and control surfaces. b,c) K_D's were calculated using a one-site binding model, $Y = B_{max}*X/(K_D + X)$. Dose–response curves were performed in triplicate, and the error bars are SEM. NB = no binding.

FL, a 2- to 10-fold increase in affinity was observed (Figure 3). However, a construct consisting of only the KS domain of PikAIV (without its docking domain) did not bind to PikAIII ACPdd-FL (data not shown). Most likely, the presence of downstream domains in these longer constructs stabilizes the productive binding conformation of the PikAIV KSdd. Furthermore, it is possible that additional protein–protein contacts exist between the upstream ACPdd and the downstream KS-AT region of the module, although these regions have yet to be identified (*10, 22*).

Our *in vitro* binding affinities for these canonical modular PKS docking domains are similar to those measured by SPR and ITC for the orthogonal discrete TubB/TubC docking elements (K_D ~50 μM), domains found in some mixed-PKS-NRPS synthetases, whose novel structure was reported recently (*28*). Additionally, the affinity of the PikAIV full module for PikAIII ACPdd as assessed by fluorescence polarization (5 ± 1 μM) is comparable to that estimated for the DEBS 1/DEBS module 3+TE obtained by monitoring rates of tri- and tetraketide lactone synthesis (2.6 μM) *in vitro* (*32*). Thus, correct pairing of large multidomain modules in both PKS and mixed PKS-NRPS biosynthetic assembly lines appears to result, at least in part, from specificity determinants with rather weak affinities. Despite these weak affinities, discrete docking domains from the related phoslactomycin (Plm) biosynthetic cluster have been used to separate the trimodular PikAI PKS (Figure 1, panel b) into monomodular proteins in a *Streptomyces venezuelae* strain lacking *pikAI* (J. Yan, S. Gupta, DHS, KAR, unpublished results). Remarkably, generation of the final macrolide products (methymycin and pikromycin) were within 2-fold of the total yield compared with production when using native PikAI. How the bacteria achieve such exquisite selectivity albeit with only modest protein–protein affinities remains poorly understood. However, one clue might come from the analysis of the PksX

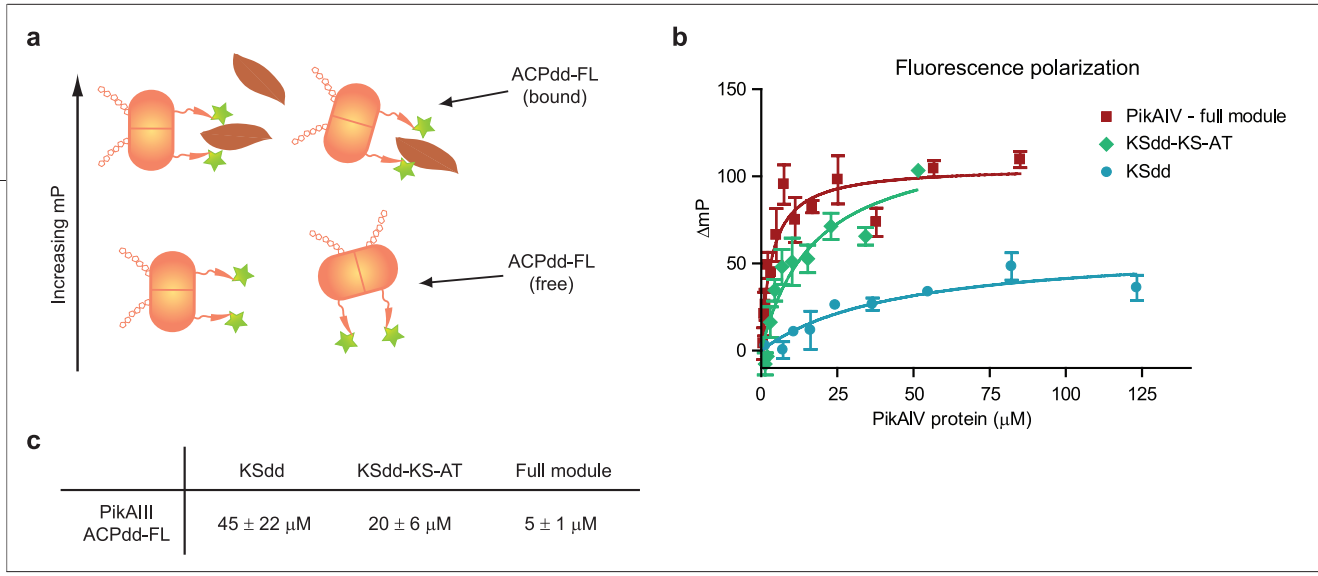

c

	KSdd	KSdd-KS-AT	Full module
PikAIII ACPdd-FL	45 ± 22 μM	20 ± 6 μM	5 ± 1 μM

Figure 3. Binding analysis of fluorescent PikAIII ACPdd to PikAIV KSdd-containing proteins measured by fluorescence polarization. a) FP assay design: 50 nM PikAIII ACPdd-FL was mixed with varying concentrations of KSdd, KSdd-KS-AT, or full module PikAIV and allowed to equilibrate at RT before reading. b,c) K_D's were calculated using a one-site binding model, $Y = B_{max}*X/(K_D + X)$. Dose response curves were performed in triplicate, and the error bars are SEM.

megacomplex, a mixed PKS-NRPS responsible for producing bacillaene. In this system, the proteins of the biosynthetic machinery have been visualized *via* fluorescence microscopy to reside at a single organelle-like complex in the bacteria, perhaps suggesting that higher order multivalent interactions are available to further increase the affinities if needed (*33*).

Structure of the PikAIII/PikAIV Docking Interface. We next explored the structural basis for the observed binding specificity between the discrete pikromycin and erythromycin docking domain pairs. Given the low sequence similarity between the structurally characterized H1-T1 class and the uncharacterized H2-T2 class of PKS docking domains, we targeted the recently proposed H2-T2 class for structure determination (*24*). A direct fusion strategy had been used successfully to generate a construct to solve the DEBS 2/DEBS 3 solution structure (*18*). To characterize the low-affinity PikAIII/PikAIV docking domain complex, we generated constructs where the C-terminus of PikAIII ACPdd was either directly fused to the N-terminus of PikAIV KSdd or separated by one or two Gly-Gly-Gly-Ser spacers. In the PikAIII/PikAIV system, this docking domain fusion strategy yielded proteins that were highly soluble, and purification yielded 25−75 mg protein L^{-1} of culture (data not shown). Docking domain constructs derived from PikAIII/PikAIV containing all four predicted helices eluted as two oligomeric species on size exclusion chromatography, but these proteins failed to form crystals. This is likely due to the existence of mobile linker regions, as were found in the DEBS 2/DEBS 3 docking complex (*18*). We then targeted a smaller construct focused only on the putative interpolypeptide docking helices (amino acids 1534−1562 of PikAIII ACPdd fused to amino acids 1−37 of the KSdd of PikAIV, together termed P3P4dock) (Figure 4). The P3P4dock crystal structure was solved by single wavelength anomalous diffraction using selenomethionyl protein. The 1.75 Å crystal structure of P3P4dock includes residues 1544−1562 of PikAIII ACPdd and 1−37 of PikAIV KSdd, whereas residues 1534−1543 were disordered and remain unresolved.

The P3P4dock protein structure consists of a short helix bound to a parallel coiled-coil (Figure 4, panels b and c) (*18*). The relevant docking interface is made up of a coiled-coil of a single homodimer flanked by two individual ACPdd helices from neighboring protein molecules in the crystal lattice (Figure 4, panel b and Supplementary Figure 5). The coiled-coil packing exhibits the familiar heptad repeat architecture with the "a" and "d" amino acids forming the core of the coiled-coil and the "e" and "g" positions providing the majority of the residues for contacting the upstream PiKAIII ACPdd helix (Supplementary Figure 5, panels d−f). The dominant interaction of the PikAIII ACPdd helix occurs in a hydrophobic patch on the PikAIV KSdd coiled-coil (Supplementary Figure 5, panels b and c). The interacting hydrophobic surfaces display exquisite shape complementarity (Figure 5). Additional interdomain interactions are found where residues 1544−1547 of PikAIII ACPdd fold back to interact further downstream on the KSdd dimer (Figure 5, panels a and b). This positioning of residues 1544−1547 in PikAIII ACPdd is mediated by a charge−charge interaction between Asp1545 of PikAIII and Lys17 of PikAIV, as well as hydrogen bonds between main chain carbonyls from Ile1544 and Leu1547

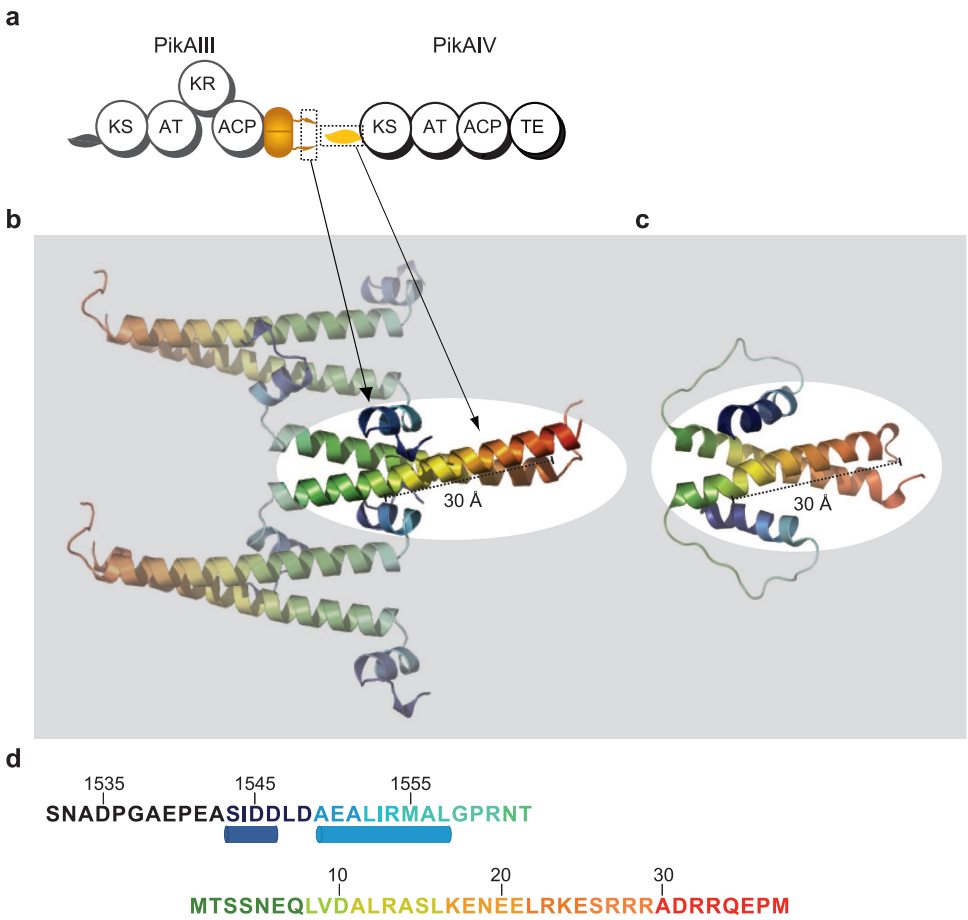

Figure 4. PKS docking interface structures. a,b) Packing of the PikAIII ACPdd/PikAIV KSdd crystal structure (PDB id 3F5H). Three P3P4dock dimers are shown. The docking interaction formed by neighboring dimers is highlighted. c) In the NMR structure of the DEBS 2 ACPdd—DEBS 3 KSdd (PDB id 1PZR), the docking interaction is intramolecular. In panels b and c, polypeptide chains are colored blue to red from the N-terminus to the C-terminus of the construct. d) P3P4dock sequence; top line is residual purification tag (SN) followed by PikAIII (residues 1534—1562), bottom line is PikAIV (residues 1—37). ACPdd are indicated below the sequence.

of PikAIII and Arg13 of PikAIV (Figure 5, panel a). No other charge—charge interactions are seen at the PikAIII/PikAIV docking interface. These electrostatic interactions and remarkable shape complementarity represent a potential selectivity filter (Figure 4, panel d).

The PikAIII/PikAIV docking domain structure revealed an overall architecture similar to that of the DEBS 2/DEBS 3 docking domain model obtained *via* NMR spectroscopy (Figure 4, panels b and c) (*18*). In both the PikAIII/PikAIV and DEBS 2/DEBS 3 docking domain structures, the ACPdd helix binds to the KSdd coiled-coil approximately 30 Å (Figure 4, panel a) from the downstream KS catalytic domain (not present in either structure). However, many details of the structures differ. The most apparent structural difference between the PikAIII/PikAIV and DEBS 2/DEBS 3 docking domains is the length of the terminal ACPdd helix (Figures 4 and 5). The 9-residue PikAIII ACPdd helix (residues 1549—1557) is considerably shorter than its 15-residue DEBS 2 ACPdd counterpart. Although both the PikAIII/PikAIV and DEBS 2/DEBS 3 docking domain interfaces display well-defined shape complementarity between matched

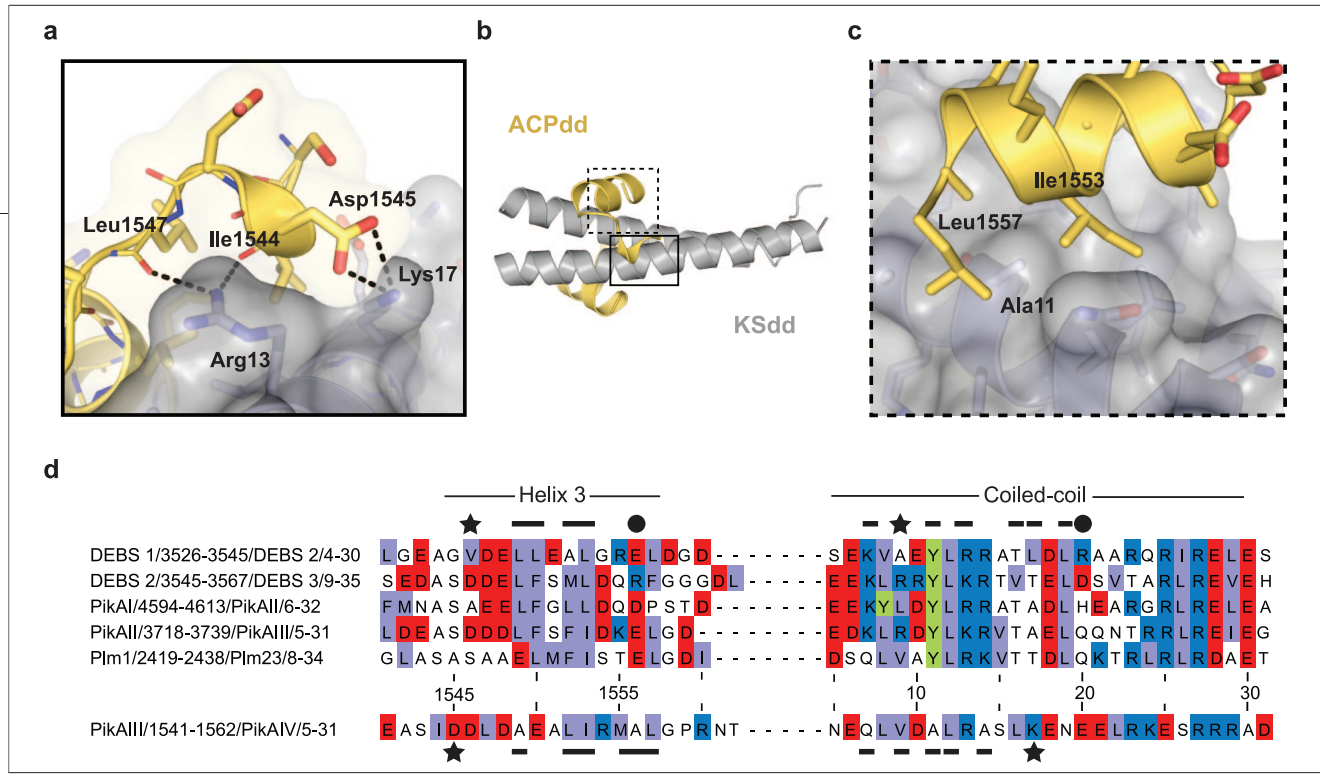

Figure 5. Shape complementarity in PKS docking domains. a—c) Docking interface of PikAIII-PikAIV; KSdd of PikAIV is colored gray, and the terminal helix of PikAIII ACPdd is light yellow. d) Multiple sequence alignment of the docking domains tested (or highlighted) in this study generated in JalView. Residue numbering is shown for the PikAIII/PikAIV pairing. Basic residues are colored dark blue, acidic residues are red, hydrophobic amino acids are light blue, and tyrosine is highlighted in green. Regions of interaction for each subclass are denoted by matching symbols.

pairs, the mis-matched pairs appear highly noncomplementary. Polar interactions also differ between the two interfaces.

The classification of PKS docking domains proposed by Thattai *et al.* (*24*) is generally consistent with the two experimental structures of paired docking domains in which DEBS 2/DEBS 3 is type H1-T1 and PikAIII/PikAIV is type H2-T2 (Figure 5, panel d). For example, the residues analogous to PikAIII Asp1545 and PikAIV Lys17 of the H2-T2 subclass are most frequently an Asp/Lys pair. In contrast, small or hydrophobic residues occupy those positions in the H1-T1 subclass of PKS docking domains (Figure 5, panel d and Supplementary Figure 6). In addition, the key residues involved in the hydrophobic interface are shifted between the proposed H1-T1 and H2-T2 subclasses of PKS docking domains (see bars above the sequence alignments in Figure 4, panel d). Furthermore, residue 11 is an alanine in PikAIV and all other H2-T2 KSdd's, whereas in over 90% of H1-T1 KSdd's the analogous residue is a tyrosine (*24*) (Figure 5 and Supplementary Figure 6). On the ACPdd helix, the large hydrophobic residues Ile1553 and Leu1557 are across the interface from Ala11 of PikAIV KSdd (Figure 5, panel c). Because of the size of these residues on the ACPdd helix, accommodating the tyrosine side chain of an H1-T1 KSdd at the position analogous to Ala11 of PikAIV KSdd appears unfavorable and likely represents another selectivity filter between the H1-T1 and H2-T2 subclasses. Altogether, these data lend support to the hypothesis that H1-T1 and H2-T2 are structurally distinct subclasses of PKS docking domains.

Specificity within the H1-T1 class appears to be driven by three distinct interaction zones. The hydrophobic core of the protein—protein interface is symbolized (Figure 5, panel d) by solid bars above both the ACPdd and the KSdd in the multiple sequence alignment. On either side of the hydrophobic core are positions of potential charge—charge interaction (Figure 5, panel d, stars and circles). Mismatching at any of the three zones appears to be sufficient to inhibit noncognate docking domains from binding productively to one another *in vitro*. For example, at the "star" position, the DEBS 2/DEBS 3 pair and the PikAII/PikAIII pair both contain the same attractive charge—charge pair (Asp/Arg). However, at the "circle" position, a mismatched PikAII/DEBS 3 pairing would bring two negatively charged residues (Glu/Asp) in close proximity. A report of productive association and transfer between PiKAII and DEBS 3 *in vivo* suggests that within the H1-T1 class, interpolypeptide interactions beyond the docking domains may also come into play (*16*), although further structural work is needed to identify additional contact regions.

An increased understanding of the key steps involved in PKS-mediated intermodular acyl group transfer provides several exciting opportunities. As the num-

ber of orphan noncollinear biosynthetic clusters rises with the completion of microbial genome sequencing projects, the ability to sequentially order the polypeptides *via* prediction of docking domain compatibility could enable more facile prediction of core polyketide structures. Combined with the predictive tools already in place for PKS catalytic domains, this enhanced analytical power should enable more accurate assignment of individual pathway metabolic products. The ultimate goal is to design and build hybrid PKS systems utilizing heterologous module pairs in a combinatorial fashion. To achieve more efficient polyketide production and the generation of novel drug-like products, we will be required to combine the lessons learned for optimizing key protein−protein interactions at the interpolypeptide interface and those related to identification of catalytic domains capable of processing non-native substrates.

METHODS

Design of Expression Constructs. Plasmids for the expression of the discrete docking domain fragments, PikAIV KSdd-KS-AT, and the full module of PikAIV were generated by amplification using PCR with LIC overhangs and inserted into the vector pMCSG7 (*34*). DEBS 1, DEBS 2, and DEBS 3 docking domains were amplified from cosmid pDHS9746. PikAI ACPdd and KSdd were amplified from plasmid pDHS0030. PikAII ACPdd and KSdd were amplified from plasmid pDHS0805. PikAIII ACPdd, PikAIII ACPdd-C-FL and KSdd were amplified from plasmid pDHS8011. PikAIV KSdd, KSdd-KS-AT, and the full module were amplified from plasmid pDHS0137. All primers are listed in Supplementary Table 1. All PCR fragments were inserted in the vector pMCSG7 *via* ligation independent cloning. Similarly, a construct lacking the N-terminal docking domain, termed PikAIV KS, was amplified from plasmid pDHS0137 and inserted into pMocr (*35*). The C-terminus of the PikAIV discrete ketosynthase construct terminates at a position near that of a recently reported soluble DEBS module 3 KS (*36*).

A plasmid encoding the full PikAIII ACPdd fused to the PikAIV KSdd (pDHS9672) was generated *via* sequential PCR amplification of (i) individual dd's PikAIII and PikAIV containing appropriate overlapping DNA at the ends using plasmid DNA for PikAIII (pDHS8011) and PikAIV (pDHS0137) and (ii) the fused construct from PCR amplification of the combined fragments using outside primers. The plasmid pDHS9570 (encoding P3P4dock) was generated by PCR amplification of a fragment of pDHS9672 followed by insertion into the vector pMCSG7. All DNA sequences were confirmed by sequencing.

Expression and Purification of Docking Domain Proteins. Plasmids encoding TEV protease-cleavable N-terminal His_6-fusion proteins were transformed into *E. coli* BL21(DE3) and grown at 37 °C in TB medium to an OD_{600} of ~1.0 in 2-L flasks. The cultures were cooled to 18 °C, and isopropyl β-D-thiogalactopyranoside was added to a final concentration of 0.2 mM and grown for 12−16 h with shaking. The cells were harvested by centrifugation and frozen at either −20 or −80 °C. Selenomethionyl protein was produced in a similar fashion using selenomethionine minimal medium (*37*). Cell pellets were thawed to 4 °C and resuspended in 5X volume of lysis buffer (20 mM HEPES, pH 7.8, 300 mM NaCl, 20 mM imidazole, 1 mM $MgCl_2$, and ~100 mg CelLytic Express (Sigma-Aldrich)) before lysis *via* sonication. For discrete KSdd's, Complete Protease Inhibitor Cocktail tablets (Roche) were added to the lysis buffer. Centrifugation at 25,000 × *g* for 30 min provided clarified lysates. Proteins were purified using Ni-Sepharose affinity chromatography on an Akta FPLC. Briefly, after filtration of the supernatant through a 0.45 μm membrane, the solution was loaded onto a 5-mL HisTrap nickel-nitrilotriacetic acid column. The column was washed with 10 column volumes of buffer A (20 mM HEPES, pH 7.8, 300 mM NaCl, 20 mM imidazole) and eluted with a linear gradient of buffer B (20 mM HEPES, pH 7.8, 300 mM NaCl, 400 mM imidazole). His-tag removal was achieved by TEV protease incubation overnight at 4 °C in HEPES buffered saline (20 mM HEPES, pH 7.8, 150 mM NaCl, HBS) or buffer A containing 1 mM TCEP. His-tagged peptides and TEV protease were removed by repassaging the solution over the HisTrap column. Flow-through fractions were pooled, concentrated, and loaded onto a HiLoad 16/60 Superdex 75 (GE Healthcare) column equilibrated with HBS. Fractions were combined, concentrated, frozen, and stored at −80 °C. Because many of the small peptides lack amino acids with appreciable absorbance at 280 nm, protein concentration was determined using the bicinchoninic acid (BCA) method using BSA as a standard. Protein yields varied from 1−75 mg L^{-1} of cell culture. PikAII and PikAIII KSdd were chemically synthesized by Genscript Corp. Proteins were further purified by size exclusion chromatography on the HiLoad 16/60 Superdex 75 as above to remove residual HPLC purification contaminants before using the peptides in binding assays. To ensure that no undesired cleavage products were formed during TEV protease incubation, the PikAIV, DEBS 2, and DEBS 3 KSdd's were subjected to high resolution mass spectrometry (data not shown). For each peptide, the observed molecular weight was consistent with cleavage exclusively at the predicted TEV protease site (Supplementary Figure 1).

Expression and Purification of PikAIV KS, PikAIV KSdd-KS-AT, and PikAIV Full Module. Proteins were expressed as described for the docking domains above except that the PikAIV full module construct was grown in BAP1 *E. coli* cells (*38*) to provide post-translational modification of its ACP domain. Proteins were purified as above using the following buffers. For cell lysis, lysis buffer with reductant (20 mM HEPES, pH 7.8, 300 mM NaCl, 20 mM imidazole, 0.5 mM TCEP 1 mM $MgCl_2$, and ~100 mg CelLytic Express) was used. During FPLC purification, wash buffer was buffer C (20 mM HEPES, pH 7.8, 300 mM NaCl, 20 mM imidazole, 10% glycerol, 0.5 mM TCEP), and the elution buffer used was buffer D (20 mM HEPES, pH 7.8, 300 mM NaCl, 400 mM imidazole, 10% glycerol, 0.5 mM TCEP). Size exclusion chromatography was performed on a HiLoad 16/60 Superdex 200 (GE Healthcare) column equilibrated with storage buffer (20 mM HEPES, pH 7.5, 150 mM NaCl, 10% glycerol, 0.5 mM TCEP). Protein concentrations were determined using absorbance at 280 nm and calculated extinction coefficients (PikAIV KS, 1 A_{280} = 1.0 mg mL^{-1}; PikAIV KSdd-KS-AT, 1 A_{280} = 0.91 mg mL^{-1}; PikAIV full module, 1 A_{280} = 0.94 mg mL^{-1}) (Supplementary Figure 1).

Surface Plasmon Resonance Assays. Sensor chips (NTA) and HBS-P buffer were purchased from GE Healthcare Life Sciences. SPR experiments were performed on a BIAcore 3000 instrument. Running buffer for SPR was HBS-P+E (10 mM HEPES, pH 7.4, 0.15 M NaCl, 0.005% surfactant P20, 50 μM EDTA). The surface was prepared for immobilization of ACPdd by activating with

TABLE 1. Diffraction Data

Parameter	Native	SeMet
Space group	$C222_1$	$C222_1$
Dimensions (Å) *a*, *b*, *c*	59.0, 117.9, 41.8	59.7, 118.5, 41.9
X-ray source	APS 23ID-D	APS 23ID-D
Wavelength λ (Å)	0.97934	0.97940
d_{min} (Å)[a]	1.75 (1.81−1.75)	2.80 (2.90−2.80)
Unique observations	15,084	3,917
R_{merge} (%)[a,b]	6.9 (50.7)	12.3 (29.7)
$\langle I/\sigma \rangle$[a]	15.6 (2.1)	11.5 (4.3)
Completeness (%)[a]	99.2 (98.0)	100 (100)
Av redundancy[a]	3.6 (3.1)	5.1 (5.1)

[a]Values in parenthesis are for outer shell [b]$R_{merge} = \Sigma|I_i - \langle I \rangle|/\Sigma I_i$, where I_i is the intensity of the *i*th observation and $\langle I \rangle$ is the mean intensity.

12 μL of 500 μM $NiCl_2$ in HBS-P. Both the loading concentration and contact time were empirically determined for each ACPdd so that the maximum amount of protein was immobilized on the chip and that this protein was stably bound for the course of the experiment. ACPdd concentrations used for loading varied depending on the protein between 50 nM and 1 μM. Typically, 700−1500 RU of ACPdd was bound to the Ni-NTA sensor chip for each experiment. To measure binding to ACPdd by SPR, solutions of KSdd in HBS-P+E were injected over the prepared surface as well as a nickel-only flow cell at a flow rate of 10 μL min^{-1}. After multiple injections (8−10 concentrations), the surface was regenerated using 30 μL of 175 mM EDTA in HBS-P, pH 8.3. Maximum testable concentrations for the KSdd's were limited by either the solubility of the peptide or its level of nonspecific binding to the nickel-only control lane. Kinetic data analysis was carried out using Scrubber2 (BioLogic Software) and BIAevaluation (GE Healthcare Life Sciences). Nonlinear curve fitting of the equilibrium binding response was carried out using GraphPad Prism software. Error shown is standard error of the mean (SEM).

Fluorescence Polarization Assays. Labeled ACPdd's were generated by reaction of BODIPY FL C_1-IA (*N*-(4,4-difluoro-5,7-dimethyl-4-bora-3a,4a-diaza-*s*-indacene-3-yl)methyl) iodoacetamide) (Invitrogen) with cysteine-containing ACPdd's. Briefly, 4 μL of 100 mM TCEP in water and 40 μL of 10 mM BODIPY FL C_1-IA in DMSO were added to 360 μL of 500 μM ACPdd in HBS. Reactions were protected from light and proceeded for 2 h at room tempetature. Unreacted BODIPY FL C_1-IA was removed from the labeled protein by passing the mixture over a preequilibrated Zeba spin desalting column (Pierce) and dialyzing into HBS. FP assays were performed at 20 μL total volume in a low volume black opaque polystyrene plate (Matrix Technologies). Proteins (50 nM PikAIII ACPdd-FL tracer and varying concentrations of unlabeled KSdd-containing PikAIV constructs) were allowed to incubate together for 10 min at RT in HBS-P (10 mM HEPES, pH 7.4, 0.15 M NaCl, 0.005% surfactant P20). Fluorescence polarization measurements were made at high sensitivity setting on a SpectraMax M5 (Molecular Devices) using 485 nm excitation, 538 nm emission, and 530 nm cutoff filter. The *G* factor was determined experimentally by setting a standard of 50 nM fluorescein in 0.1 N NaOH to 20 mP. Nonlinear curve fitting of the equilibrium binding response was carried out using GraphPad Prism software. Control experiments using up to 1 mg mL^{-1} BSA confirmed that the polarization increase upon incubation of PikAIII ACPdd-FL with unlabeled PikAIV KSdd was due to a specific protein−protein interaction (data not shown).

Crystallization, Data Collection, and Structure Determination. Initial screening with P3P4dock produced small crystals of needle morphology under a variety of conditions containing high concentrations of organic solvents such as dioxane and MPD. The best-diffracting native crystals grew in 4−8 weeks at 4 °C using hanging-drop vapor diffusion techniques. Similarly, selenomethionyl P3P4dock crystals grew in 1−2 weeks at 4 °C after microseeding with native crystals. For crystal growth, an equal volume of protein solution (2.5−5 mg mL^{-1}) in HBS (20 mM HEPES, pH 7.8, 150 mM NaCl) was mixed with mother liquor containing 55% 2-methyl-2,4-pentanediol (MPD), 150−200 mM sodium acetate, pH 5.0. The crystals were harvested in loops and

TABLE 2. Refinement statistics

	PDB id 3F5H
Date range	50−1.75
R/R_{free}[a,b]	0.201/0.250
rmsd bond length (Å)	0.011
rmsd bond angle (deg)	1.216
Av protein B-factor (Å^2)	24.4
Av solvent B-factor (Å^2)	39.5
Wilson B (Å^2)	20.3
Ramachandran plot[c]	
Favored	100
Allowed	0.0
Disallowed	0.0
Protein atoms	919
Water molecules	151
Other atoms	1

[a]$R = \Sigma||F_o| - |F_c||/\Sigma|F_o|$ where F_o is the observed structure factor and F_c is the calculated structure factor used in the refinement. [b]$R_{free} = \Sigma||F_o| - |F_c||/\Sigma|F_o|$ where F_o is the observed structure factor and F_c is the calculated structure factor from 5% of reflections not used in the refinement [c]From output of MOLProbity (*45*).

frozen in liquid N_2. Diffraction data were collected at 100 K on GM/CA-CAT beamlines 23ID-B and 23ID-D at the Advanced Photon Source in the Argonne National Laboratory (Argonne, IL). The data were processed using the HKL2000 suite (*39*). Initial phasing by the single-wavelength anomalous diffraction (SAD) method was performed using data collected at the wavelength with strongest anomalous signal from a single selenomethionyl-labeled protein crystal (Table 1). To minimize radiation damage, the data set was assembled from 45° wedges of data collected from multiple points along a single crystal using a 10-μm X-ray beam (*40*). The PHENIX software package located five of the six selenium atoms and approximately two-thirds of the structure was automatically built from the 3.0 Å SAD-phased map (*41*). Two molecules were present in the asymmetric unit (V_m = 2.40, 49% solvent). Modeling was completed manually using COOT (*42*). The model was refined against the 1.75 Å native data set using REFMAC5 of the CCP4 suite (*43*–*45*) (Tables 1 and 2).

Sequence and Structure Analysis. Multiple sequence alignments were performed using the ClustalX method within JalView software (*46*). Structural figures were generated with PyMOL (DeLano Scientific).

Accession Codes: The atomic coordinates of the PikAIII/PikAIV complex have been made publicly available through the Protein Data Bank (www.rcsb.org/pdb) with the PDB id 3F5H.

Acknowledgment: The authors thank C. Rath for assistance with mass spectrometry analysis of KSdd's. BAP1 *E. coli* cells were a generous gift from C. Khosla (Stanford University). This work was funded by NIH grant R01 GM076477 and the H. W. Vahlteich Professorship (to D.H.S.) and by NIH grant R37 DK042303 (to J.L.S.). GM/CA CAT has been funded in whole or in part with federal funds from the National Cancer Institute (Y1-CO-1020) and the National Institute of General Medical Science (Y1-GM-1104). Use of the Advanced Photon Source was supported by the U.S. Department of Energy, Basic Energy Sciences, Office of Science, under contract DE-AC02-06CH11357.

Supporting Information Available: This material is available free of charge *via* the Internet.

REFERENCES

1. Hill, A. M. (2006) The biosynthesis, molecular genetics and enzymology of the polyketide-derived metabolites, *Nat. Prod. Rep. 23*, 256–320.
2. Shen, B. (2003) Polyketide biosynthesis beyond the type I, II and III polyketide synthase paradigms, *Curr. Opin. Chem. Biol. 7*, 285–295.
3. Newman, D. J., and Cragg, G. M. (2007) Natural products as sources of new drugs over the last 25 years, *J. Nat. Prod. 70*, 461–477.
4. Maier, T., Jenni, S., and Ban, N. (2006) Architecture of mammalian fatty acid synthase at 4.5 Å resolution, *Science 311*, 1258–1262.
5. Smith, S., and Tsai, S. C. (2007) The type I fatty acid and polyketide synthases: a tale of two megasynthases, *Nat. Prod. Rep. 24*, 1041–1072.
6. Tang, Y., Kim, C.-Y., Mathews, I. I., Cane, D. E., and Khosla, C. (2006) The 2.7-angstrom crystal structure of a 194-kDa homodimeric fragment of the 6-deoxyerythronolide B synthase, *Proc. Natl. Acad. Sci. U.S.A. 103*, 11124–11129.
7. Khosla, C., Tang, Y., Chen, A. Y., Schnarr, N. A., and Cane, D. E. (2007) Structure and mechanism of the 6-deoxyerythronolide B synthase, *Annu. Rev. Biochem. 76*, 11.11–11.27.
8. Fischbach, M. A., and Walsh, C. T. (2006) Assembly-line enzymology for polyketide and nonribosomal peptide antibiotics: logic, machinery, and mechanisms, *Chem. Rev. 106*, 3468–3496.
9. Reeves, C. D., Murli, S., Ashley, G. W., Piagentini, M., Hutchinson, C. R., and McDaniel, R. (2001) Alteration of the substrate specificity of a modular polyketide synthase acyltransferase domain through site-specific mutations, *Biochemistry 40*, 15464–15470.
10. Weissman, K. J., and Müller, R. (2008) Protein-protein interactions in multienzyme megasynthetases, *ChemBioChem 9*, 826–848.
11. Tsuji, S. Y., Cane, D. E., and Khosla, C. (2001) Selective protein-protein interactions direct channeling of intermediates between polyketide synthase modules, *Biochemistry 40*, 2326–2331.
12. Worthington, A. S., Hur, G. H., Meier, J. L., Cheng, Q., Moore, B. S., and Burkart, M. D. (2008) Probing the compatibility of type II ketosynthase-carrier protein partners, *ChemBioChem 9*, 2096–2103.
13. Menzella, H. G., and Reeves, C. D. (2007) Combinatorial biosynthesis for drug development, *Curr. Opin. Microbiol. 10*, 238–245.
14. Menzella, H. G., Carney, J. R., and Santi, D. V. (2007) Rational design and assemby of synthetic trimodular polyketide synthases, *Chem. Biol. 14*, 143–151.
15. Kittendorf, J. D., and Sherman, D. H. (2006) Developing tools for engineering hybrid polyketide synthetic pathways, *Curr. Opin. Biotechnol. 17*, 597–605.
16. Tang, L., Fu, H., and McDaniel, R. (2000) Formation of functional heterologous complexes using subunits from the picromycin, erythromycin and oleandomycin polyketide synthases, *Chem. Biol. 7*, 77–84.
17. Floss, H. G. (2006) Combinatorial biosynthesis—potential and problems, *J. Biotechnol. 124*, 242–257.
18. Broadhurst, R. W., Nietlispach, D., Wheatcroft, M. F., Leadlay, P. F., and Weissman, K. J. (2003) The structure of docking domains in modular polyketide synthases, *Chem. Biol. 10*, 723–731.
19. Wu, N., Tsuji, S. Y., Cane, D. E., and Khosla, C. (2001) Assessing the balance between protein-protein interactions and enzyme-substrate interactions in the channeling of intermediates between polyketide synthase modules, *J. Am. Chem. Soc. 123*, 6465–6474.
20. Wu, N., Cane, D. E., and Khosla, C. (2002) Quantitative analysis of the relative contributions of donor acyl carrier proteins, acceptor ketosynthases, and linker regions to intermodular transfer of intermediates in hybrid polyketide synthases, *Biochemistry 41*, 5056–5066.
21. Kumar, P., Li, Q., Cane, D. E., and Khosla, C. (2003) Intermodular communication in modular polyketide synthases: structural and mutational analysis of linker mediated protein-protein interactions, *J. Am. Chem. Soc. 125*, 4097–4102.
22. Weissman, K. J. (2006) Single amino acid substitutions alter the efficiency of docking in modular polyketide biosynthesis, *ChemBioChem 7*, 1334–1342.
23. Weissman, K. J. (2006) The structural basis for docking in modular polyketide biosynthesis, *ChemBioChem 7*, 485–494.
24. Thattai, M., Burak, Y., and Shraiman, B. I. (2007) The origins of specificity in polyketide protein interactions, *PLoS Comput. Biol. 3*, 1827–1835.
25. Xue, Y., Zhao, L., Liu, H. W., and Sherman, D. H. (1998) A gene cluster for macrolide antibiotic biosynthesis in *Streptomyces venezuae*: architecture of metabolic diversity, *Proc. Natl. Acad. Sci. U.S.A. 95*, 12111–12116.
26. Myszka, D. G. (2000) Kinetic, equilibrium, and thermodynamic analysis of macromolecular interactions with BIACORE, *Methods Enzymol. 323*, 325–340.
27. Papalia, G. A., Leavitt, S., Bynum, M. A., Katsamba, P. S., Wilton, R., Qiu, H., Steukers, M., Wang, S., Bindu, L., Phogat, S., Giannetti, A. M., Ryan, T. E., Pudlak, V. A., Matusiewicz, K., Michelson, K. M., Nowakowski, A., Pham-Baginski, A., Brooks, J., Tieman, B. C., Bruce, B. D., Vaughn, M., Baksh, M., Cho, Y. H., Wit, M. D., Smets, A., Vandersmissen, J., Michiels, L., and Myszka, D. G. (2006) Comparative analysis of 10 small molecules binding to carbonic anhydrase II by different investigators using Biacore technology, *Anal. Biochem. 359*, 94–105.

28. Richter, C. D., Nietlispach, D., Broadhurst, R. W., and Weissman, K. J. (2008) Multienzyme docking in hybrid megasynthetases, *Nat. Chem. Biol. 4*, 75–81.
29. Nieba, L., Nieba-Axmann, S. E., Persson, A., Hämäläinen, M., Edebratt, F., Hansson, A., Lidholm, J., Magnusson, K., Karlsson, Å. F., and Plückthun, A. (1997) BIACORE analysis of histidine-tagged proteins using a chelating NTA sensor chip, *Anal. Biochem. 252*, 217–228.
30. Kittendorf, J. D., Beck, B. J., Buchholz, T. J., Seufert, W., and Sherman, D. H. (2007) Interrogating the molecular basis for multiple macrolactone ring formation by the pikromycin polyketide synthase, *Chem. Biol. 14*, 944–954.
31. Owicki, J. C. (2000) Fluorescence polarization and anisotropy in high throughput screening: perspectives and primer, *J. Biomol. Screen. 5*, 297–306.
32. Gokhale, R. S., Hunziker, D., Cane, D. E., and Khosla, C. (1999) Mechanism and specificity of the terminal thioesterase domain from the erythromycin polyketide synthase, *Chem. Biol. 6*, 117–125.
33. Straight, P. D., Fischbach, M. A., Walsh, C. T., Rudner, D. Z., and Kolter, R. (2007) A singular enzymatic megacomplex from *Bacillus subtilis*, *Proc. Natl. Acad. Sci. U.S.A. 104*, 305–310.
34. Stols, L., Gu, M., Dieckman, L., Raffen, R., Collart, F. R., and Donnelly, M. I. (2002) A new vector for high-throughput, ligation-independent cloning encoding a tobacco etch virus protease cleavage site, *Protein Expression Purif. 25*, 8–15.
35. Delproposto, J., Majmudar, C. Y., Smith, J. L., and Brown, W. C. (2009) Mocr: A novel fusion tag for enhancing solubility that is compatible with structural biology applications, *Protein Expression Purif. 63*, 40–49.
36. Chen, A. Y., Cane, D. E., and Khosla, C. (2007) Structure-based dissociation of a type I polyketide synthase module, *Chem. Biol. 14*, 784–792.
37. Guerrero, S. A., Hecht, J.-J., Hofmann, B., Biebl, H., and Singh, M. (2001) Production of selenomethionine-labelled proteins using simplified culture conditions and generally applicable host/vector systems, *Appl. Microbiol. Biotechnol. 56*, 718–723.
38. Pfeifer, B. A., Admiraal, S. J., Gramajo, H., Cane, D. E., and Khosla, C. (2001) Biosynthesis of complex polyketides in a metabolically engineered strain of *E. coli*, *Science 291*, 1790–1792.
39. Otwinowski, Z., and Minor, W. (1997) Processing of X-ray diffraction data collected in oscillation mode, *Macromol. Crystallogr., A 276*, 307–326.
40. Sanishvili, R., Nagarajan, V., Yoder, D., Becker, M., Xu, S., Corcoran, S., Akey, D. L., Smith, J. L., and Fischetti, R. F. (2008) A 7 micron mini-beam improves diffraction data from small or imperfect crystals of macromolecules, *Acta Crystallogr. Sect. D Biol. Crystallogr. 64*, 425–435.
41. Adams, P. D., Grosse-Kunstleve, R. W., Hung, L. W., Ioerger, T. R., McCoy, A. J., Moriarty, N. W., Read, R. J., Sacchettini, J. C., Sauter, N. K., and Terwilliger, T. C. (2002) PHENIX: building new software for automated crystallographic structure determination, *Acta Crystallogr., Sect. D: Biol. Crystallogr. 58*, 1948–1954.
42. Emsley, P., and Cowtan, K. (2004) Coot: model-building tools for molecular graphics, *Acta Crystallogr., Sect. D: Biol. Crystallogr. 60*, 2126–2132.
43. Murshudov, G. N., Vagin, A. A., and Dodson, E. J. (1997) Refinement of macromolecular structures by the maximum-likelihood method, *Acta Crystallogr., Sect. D: Biol. Crystallogr. 53*, 240–255.
44. Collaborative Computational Project, N. (1994) The CCP4 suite: programs for protein crystallography, *Acta Crystallogr., Sect. D: Biol. Crystallogr. 50*, 760–763.
45. Davis, I. W., Murray, L. W., Richardson, J. S., and Richardson, D. C. (2004) MOLPROBITY: structure validation and all-atom contact analysis for nucleic acids and their complexes, *Nucleic Acids Res. 32*, W615–W619.
46. Clamp, M., Cuff, J., Searle, S. M., and Barton, G. J. (2004) The Jalview Java alignment editor, *Bioinformatics 20*, 426–427.